Robust Adaptation in Dynamically Switching Load Frequency Control

by

Spandan Roy, Tian Tao, Shuai Yuan, Simone Baldi

Report No: IIIT/TR/2019/-1

Centre for Robotics
International Institute of Information Technology
Hyderabad - 500 032, INDIA
November 2019

Robust Adaptation in Dynamically Switching Load Frequency Control ⋆

Tian Tao [**] **Spandan Roy** [**,****] **Shuai Yuan** [***]
Simone Baldi [*,**]

[*] *School of Mathematics, Southeast University, Nanjing, China*
[**] *Delft Center for Systems and Control, TU Delft, The Netherlands*
[***] *Research Center of Intelligent Control and Systems, Harbin Institute of Technology, China*
[****] *Robotics Research Centre, International Institute of Information Technology Hyderabad, India (e-mails: {T.Tao-1,s.baldi}@tudelft.nl, shuaiyuan@hit.edu.cn, spandan.roy@iiit.ac.in)*

Abstract: In recent years, heuristics for adaptive solutions to load frequency control (LFC) in power systems have been proposed that include adapting the LFC targets or adapting the participation factor for the resources. However, stability guarantees for these adaptation ideas are missing, especially in the presence of switching/evolving topologies of the power system. In today's smart grids, switching topologies often arise from reconfiguration and resilience against faults or from switching among different control areas in order to dampen oscillations and face cyber attacks. This work proposes a novel LFC framework in which adaptation and switching topologies are combined in a provably stable way.

Keywords: Power systems, load frequency control, adaptive control algorithm, grid resilience, switching/evolving topologies.

1. INTRODUCTION

In power systems, randomness from the power load demand and from renewable energy sources may cause frequency oscillations among interconnected power systems. A load frequency control (LFC) achieves stability of frequency by adjusting the reference power of the governor. Nowadays, LFC is often implemented beyond single areas, i.e. it connects multiple areas of the power system, acting in conjunction with wide area damping control (Roy et al. (2018)). Therefore, LFC heavily relies on communication between sensors and energy management systems which faces a wide range of unpredictable and highly-uncertain parameters, including risks of faults or cyber-attacks. Several methodologies have been proposed for LFC and it is difficult to give a complete overview: most LFC techniques are based on fixed-gain 'robust' controllers designed for some worse-case deviations from the nominal parameters of the power system. Examples include: proportional-integral (PI) control, internal model control (Saxena and Hote (2013)), fuzzy logic control (Yousef (2015); Yousef et al. (2014)), model-predictive control (Ersdal et al. (2016)), optimal control (Zhao et al. (2014); Mallada et al. (2017)) (see also references therein).

With the presence of renewable energy systems and microgrids, the stress and the level of uncertainty in power systems goes beyond the capabilities of a robust control approach (Doolla and Bhatti (2006); Fan et al. (2009); Korkas et al. (2015); Abazari et al. (2019)), and stimulates new studies on LFC and related stability issues. For these reason, several researchers in power systems have been looking for *adaptive solutions to LFC*, where the controller is not fixed-gain, but is capable of adapting to changing circumstances: the essential concept of adaptation in LFC is to enhance and lower the controller activity by assigning weights throughout the operation (Hanwate et al. (2018)), e.g. based on the covariances between area errors (Polajžer et al. (2018)), or on the participation factors for the resources (Boonchuay (2014); Prostejovsky et al. (2018)). Unfortunately, as the proposed adaptive LFC methods are based on heuristics, a formal adaptation framework with stability guarantees is to a large extent missing. It is also important to note that interconnections in modern power systems are not fixed a priori, but can change with time (*switching topologies*). Regulating the system frequency may require coordinately switching among different control areas in order to dampen oscillations (Polajžer et al. (2018)); when frequency violates a threshold, load-side controllers can switch to a frequency regulation mode in which each controller communicates with neighboring controllers to discover power imbalances (Zhang et al. (2019)); also, tolopogies can be intentionally changed for mitigating cyber-attacks, so as to prevent load manipulation from attackers (Mahmoud et al. (2019); Schiffer et al. (2017)). All these scenarios involve the design of switching signals that continuously change the topology of the power system (Liu et al. (2016)): no adaptation LFC framework has been proposed that can handle this crucial challenge.

⋆ This work was partly supported by the Fundamental Research Funds for the Central Universities grant no. 4007019109 (RECONSTRUCT), and by the special guiding funds "double first-class" grant no. 4007019201

Manuscript 554 submitted to 21st IFAC World Congress, 2020.
Received November 8, 2019.

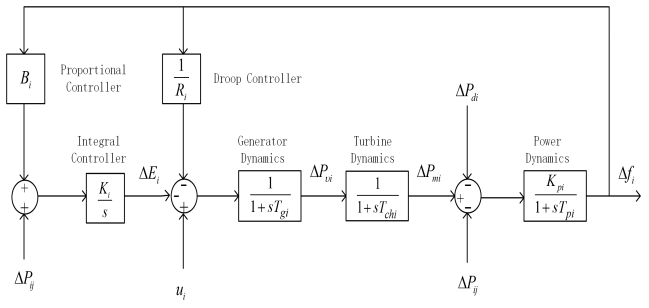

Fig. 1. Single area power system for LFC purposes

In view of the above discussion and towards the design of resilient power systems under uncertainty, this work proposes a novel LFC framework in which adaptation and switching topologies are combined in a provably stable way. Stability is studied analytically in the Lyapunov theory sense. The rest of the paper is organized as follows: Section 2 introduces the system dynamics and the problem formulation; the adaptive framework is proposed in Section 3. Simulation results are shown in Section 4. Stability proofs are in Appendix.

2. DYNAMICS AND PROBLEM FORMULATION

Before introducing a multi-area power system and its dynamics, let us recall the standard dynamics for a single-area power system (Mu et al. (2017); Dey et al. (2012)). The area is indexed with subscript i (see Fig. 1):

$$\Delta\dot{P}_{mi}(t) = \frac{\Delta P_{\nu i}(t)}{T_{chi}} - \frac{\Delta P_{mi}(t)}{T_{chi}} \tag{1a}$$

$$\Delta\dot{E}_i(t) = -k_i\Delta P_f(t) + k_i B_i \Delta f_i(t) \tag{1b}$$

$$\Delta\dot{P}_{\nu i}(t) = -\frac{\Delta f_i(t)}{R_i T_{gi}} - \frac{\Delta P_{\nu i}(t)}{T_{gi}} - \frac{\Delta E_i(t)}{T_{gi}} + \frac{u_i(t)}{T_{gi}} \tag{1c}$$

$$\Delta\dot{f}_i(t) = -\frac{k_{pi}\Delta P_{di}(t)}{T_{pi}} - \frac{k_{pi}\Delta P_{ij}(t)}{T_{pi}} + \frac{k_{pi}\Delta P_{mi}(t)}{T_{pi}} - \frac{\Delta f_i(t)}{T_{pi}} \tag{1d}$$

where all constants and variables are explained in Table 1. In (1), $\Delta P_{ij}(t)$ is the disturbance from neighboring areas (indexed by subscript j), which will be clarified in the next subsection. The Δ in front of any quantity represents the deviation from the equilibrium state of the system.

Remark 1. In this work we consider an ***uncertain power system*** *in which the exact value of all constants in* (1) *is unknown and not available for control design.*

2.1 Multi-area power system

To describe the dynamics of a multi-area power network in a more compact way, it is suitable to describe the power system as a network of dynamical systems, linked to each other via a *communication/interaction graph* that captures the allowed information flow or the allowed physical interaction: area i has an *undirected* connection to area j if the second can receive information from or physically interact with the first and vice versa. In this work we consider for simplicity a unique communication/interaction graph, although one can have two different graphs, one capturing communication flow and one physical interaction. As standard in graph theory, we consider connected graphs, i.e., a path exists between every pair of areas. For a set of areas, there might be different interconnections, or *topologies*: Fig. 2 shows a three-area power system (each node denotes one area) with 4 possible connected topologies, indexed by $\sigma \in \Omega = \{1, 2, 3, 4\}$. We use the notation $\mathcal{N}_i$ to indicate all the neighboring areas to area i: e.g. in Fig. 2, when $\sigma = 1$, area 1 has one neighbour, i.e. $\mathcal{N}_1 = \{2\}$; when $\sigma = 2$, area 1 has two neighbours, i.e. $\mathcal{N}_1 = \{2, 3\}$ and so on.

Table 1. List of symbols

n	Number of areas
N	Number of (connected) topologies
$\Delta P_{\nu i}$	Governor valve position
ΔP_{mi}	Mechanical power output of the alternator
ΔE_i	Area control error signals
ΔP_{di}	Load disturbances
Δf_i	Frequency deviations
$\Delta\theta_i$	Phase deviation
u_i	Input signal
B_i	Proportional gain of local PI control
K_i	Integral gain of local PI control
T_{pi}	Power system time constants
D_i	Generator damping coefficients
T_{gi}	Governor time constants
T_{chi}	Turbine time constants
R_i	Speed droops
T_i	Stiffness coefficients

The introduction has mentioned several reasons why topologies in power networks might evolve with time. In this work, the changing topology is represented by a piecewise constant time-dependent signal $\sigma(\cdot)$, called the *switching signal*, taking values in the topology set $\Omega := \{1, 2, \ldots, N\}$ (cf. the switching example in Fig. 3). The switching instants of $\sigma(\cdot)$ are denoted by $t_l, t_{l+1}, \cdots$, and the intervals in between switching instants are $[t_l, t_{l+1})$, $l = 1, 2, \cdots$. Accordingly, the set of neighbors of area i will be topology-dependent and denoted by $\mathcal{N}_{i\sigma(t)}$. Whenever convenient we may not explicitly write the dependence of σ on time. To represent the changing topologies orchestrated by the switching signal, the following class of switching signals is considered:

Definition 1. **Average Dwell Time (ADT)** (Hespanha and Morse (1999)): For a switching signal $\sigma(\cdot)$, let $N_\sigma(t_1, t_2)$ denote the number of discontinuities in the interval $[t_1, t_2)$. Then $\sigma(\cdot)$ has average dwell time ϑ if

$$N_\sigma(t_1, t_2) \leq N_0 + (t_2 - t_1)/\vartheta, \quad \forall t_2 \geq t_1 \geq 0$$

where $N_0 > 0$ is termed as chatter bound.

Remark 2. The class of ADT signals allows fast switching over short intervals compensated by slower switching on longer intervals (i.e. on average). This can be useful to represent situations in which fast switching occurs as a consequence of sudden events (e.g. attacks or faults), compensated by a slower settling phase.

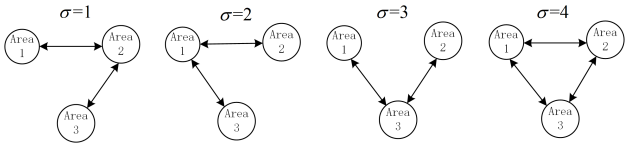

Fig. 2. Switching topologies in a three-area network

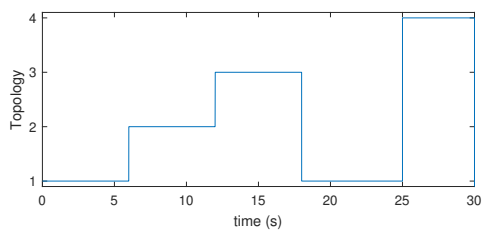

Fig. 3. A switching signal representing changing topologies

Interaction among two power-system areas i and j occurs via the differences between their phases $\Delta\theta_i$ and $\Delta\theta_j$, which creates a power flow ΔP_{ij}, according to

$$\Delta P_{ij\sigma}(t) = 2\pi T_i \sum_{j\in\mathcal{N}_{i\sigma}(t)} (\Delta\theta_i(t) - \Delta\theta_j(t)) \tag{2}$$

$$\Delta P_{ij\sigma}(t) = -\Delta P_{ji\sigma}(t) \tag{3}$$

If area j is disconnected from area i, then $\Delta P_{ij\sigma}(t) = 0$.

2.2 Switched LFC Dynamics

From (1), a second-order model can be derived using the fact that generator and turbine time constants are much smaller than power time constants (T_{gi} and T_{chi} are at least 10 times smaller than T_{pi} (Dey et al. (2012))), giving:

$$\Delta P_{mi\sigma}(t) = -\frac{\Delta f_i(t)}{R_i} + u_{i\sigma}(t) - \Delta E_{i\sigma}(t) \tag{4a}$$

$$\Delta\dot{E}_{i\sigma}(t) = -k_i\Delta P_{ij\sigma}(t) + k_i B_i \Delta f_i(t) \tag{4b}$$

$$\Delta\dot{f}_i(t) = -\frac{k_{pi}\Delta P_{di}(t)}{T_{pi}} - \frac{k_{pi}\Delta P_{ij\sigma}(t)}{T_{pi}} + \frac{k_{pi}\Delta P_{mi\sigma}(t)}{T_{pi}} - \frac{\Delta f_i(t)}{T_{pi}}, \qquad \Delta\dot{\theta}_i(t) = \Delta f_i(t) \tag{4c}$$

$$\Delta P_{ij\sigma}(t) = 2\pi T_i \sum_{j\in\mathcal{N}_{i\sigma}(t)} (\Delta\theta_i(t) - \Delta\theta_j(t)) \tag{4d}$$

We then obtain the following switched LFC dynamics:

$$\Delta\ddot{\theta}_i(t) = (-\frac{1}{T_{pi}} - \frac{k_{pi}}{T_{pi}R_i})\Delta\dot{\theta}_i - \frac{k_{pi}}{T_{pi}} 2\pi T_i \sum_{j=1}^{n} \ell_{ij,\sigma}\Delta\theta_j - \frac{k_{pi}}{T_{pi}}\big(\Delta P_{di} + \Delta E_{i\sigma}(t)\big) + \frac{k_{pi}}{T_{pi}} u_{i\sigma}(t) \tag{5}$$

where $\ell_{ij,\sigma}$ captures the topology (DeLellis et al. (2010))

$$\ell_{ij,\sigma} = \begin{cases} \|\mathcal{N}_{i\sigma}\| & \text{if } i = j \\ -1 & \text{if } (i,j) \text{ are connected} \\ 0 & \text{otherwise} \end{cases} \tag{6}$$

where $\|\mathcal{N}_{i\sigma}\|$ is the cardinality of the set $\mathcal{N}_{i\sigma}$.

Remark 3. The interest of considering a second-order model as in (5) *is to allow the use of proportional-derivative controls, commonly adopted in power systems.*

Let us define the state $x \triangleq [\Delta\theta^T \ \Delta\dot{\theta}^T]^T \in \mathbb{R}^{2n}$, with $\Delta\theta = [\Delta\theta_1, \ldots, \Delta\theta_n]^T$, $\Delta\dot{\theta} = [\Delta\dot{\theta}_1, \ldots, \Delta\dot{\theta}_n]^T$, and let us rewrite (5) and (6) in the compact form:

$$\dot{x}(t) = A_{\sigma(t)}x(t) + Bu_{\sigma(t)}(t) + d(t) \tag{7}$$

where $u_\sigma = [u_{1\sigma} \cdots u_{n\sigma}] \in \mathbb{R}^n$ is the (topology-dependent) control input; $d \in \mathbb{R}^{2n}$ is an external disturbance with unknown bound, and $\sigma(\cdot)$ is the switching signal. The switched power system (7) is uncertain as some entries of matrices $A_\sigma \in \mathbb{R}^{2n\times 2n}$ and $B \in \mathbb{R}^{2n\times n}$, $\sigma \in \Omega$ are unknown: despite uncertainty, the reader can verify from (5) that information about the structure of A_σ and B is available, e.g. A_σ contains block integrators and B is block diagonal (see the numerical example in Sect. 4).

Remark 4. According to (5)*, the disturbance in* (7) *contains the load ΔP_{di} and the unmodelled terms $\Delta E_{i\sigma}$. Robustness to unmodelled terms is an open challenge of adaptive LFC, which calls for an adaptive approach known in literature as* ***robust adaptive control*** *(Tao (2014)).*

The standard stability concept in robust adaptive control (Yuan et al. (2018)) is recalled.

Definition 2. **Uniform Ultimate Boundedness (UUB).** The switched system (7) under switching signal $\sigma(\cdot)$ is uniformly ultimately bounded if there exists a convex and compact set $\mathcal{C}$ such that for every initial condition $x(0) = x_0$, there exists a finite time $T(x_0)$ such that $x(t) \in \mathcal{C}$ for all $t \geq T(x_0)$. Further, b is said to be the ultimate bound if $\|x(t)\| \leq b$ for all $t \geq T(x_0)$.

A group of switched reference models representing the desired behavior of each topology is given as follows:

$$\dot{x}_m(t) = A_{m\sigma(t)}x_m(t) + B_{m\sigma(t)}r(t), \sigma(t) \in \Omega \tag{8}$$

where $x_m \triangleq [\Delta\theta_m^T \ \Delta\dot{\theta}_m^T]^T \in \mathbb{R}^{2n}$ is the desired state vector, and $r \in \mathbb{R}^n$ is a user-defined phase. The matrices $A_{m\sigma} \in \mathbb{R}^{2n\times 2n}$ and $B_{m\sigma} \in \mathbb{R}^{2n\times n}$ are design-driven: $A_{m\sigma}$ should be chosen Hurwitz with the same block of integrators structure of A_σ, and $B_{m\sigma}$ can be chosen in the same block diagonal structure of B_σ.

If the matrices in (7) were perfectly known, the ideal topology-dependent control that makes the power system behave like the reference models is

$$u_\sigma^*(t) = K_{\sigma(t)}^{*T}(t)x(t) + L_{\sigma(t)}^*(t)r(t) \tag{9}$$

where $K_\sigma^* \in \mathbb{R}^{2n\times n}$ and $L_\sigma^* \in \mathbb{R}^{n\times n}, \sigma \in \Omega$, are *unknown gains* satisfying the following matching conditions:

$$A_\sigma + BK_\sigma^{*T} = A_{m\sigma}, \quad BL_\sigma^* = B_{m\sigma}. \tag{10}$$

The existence of solutions to (10) is guaranteed, according to the model reference adaptive control theory (Tao (2014)), by the structure of A_σ and B, which also guarantee that L_σ^* is a diagonal positive definite matrix (see the example in Sect. 4). Since (A_σ, B) are unknown, K_σ^* and L_p^* are also unknown, so we define $K_{\sigma(t)}$ and $L_{\sigma(t)}$ as their estimates and introduce the controller

$$u_\sigma(t) = K_{\sigma(t)}^T(t)x(t) + (L_{\sigma(t)}(t) + \Gamma_{\sigma(t)}(t))r(t), \tag{11}$$

where $K_\sigma \in \mathbb{R}^{2n\times n}$, $L_\sigma \in \mathbb{R}^{n\times n}$ are to be updated from adaptive laws, and $\Gamma_\sigma = diag\{\gamma_{i\sigma}\}$, $i = 1, \cdots, m$ is an auxiliary adaptive gain to be defined later.

Let $e(t) = x(t) - x_m(t)$ be the tracking error. After substituting (11) into (7) and substracting (8), we obtain the dynamics of the tracking error as follows:

$$\dot{e}(t) = A_{m\sigma(t)}e(t) + B[\tilde{K}_{\sigma(t)}^T(t)x(t) + \big(\tilde{L}_{\sigma(t)}(t) + \Gamma_{\sigma(t)}(t)\big)r(t)] + d(t) \tag{12}$$

where $\tilde{K}_\sigma = K_\sigma - K_\sigma^*$ and $\tilde{L}_\sigma = L_\sigma - L_\sigma^*$ are the parameter estimation errors.

Control Problem: Design a multi-area LFC that can track in UUB sense the desired frequency $\Delta\dot{\theta}_m = \Delta f_m = 0$ under uncertainty and ADT switching topologies.

Manuscript 554 submitted to 21st IFAC World Congress, 2020.
Received November 8, 2019.

3. ADAPTIVE CONTROL DESIGN

This section proposes adaptive laws for the gains in (11) to solve the **Control Problem**. Correspondingly, switching laws are designed in the framework of ADT switching.

3.1 Adaptive control

Let us denote with $p \in \Omega$ the index corresponding to the active topology at time t (e.g. in the interval $t \in [t_l, t_{l+1})$), and $\overline{p} \in \mathcal{I}(p)$ to indicate the *set of inactive topologies* with respect to p. Let $P_p > 0$ be the solution to

$$A_{mp}^T P_p + P_p A_{mp} + (1+\kappa_p)P_p = -Q_p, \tag{13}$$

where κ_p, Q_p are user-defined parameters.

The adaptive law is designed, for $t \in [t_l, t_{l+1})$, as

$$\dot{K}_p^T = -S_p B_{mp}^T P_p e x^T - \delta_p S_p K_p^T,\ \dot{K}_{\overline{p}}^T = 0, \tag{14a}$$

$$\dot{L}_p = -S_p B_{mp}^T P_p e r^T - \delta_p S_p L_p,\ \dot{L}_{\overline{p}} = 0, \tag{14b}$$

$$\dot{\gamma}_{ip} = 0,$$

$$\dot{\gamma}_{i\overline{p}} = -\left(\beta_{i\overline{p}} + \delta_{\overline{p}}\left(\{K_{\overline{p}}K_{\overline{p}}^T\}_{ii} + \{L_{\overline{p}}^T L_{\overline{p}}\}_{ii}\right)\right)\gamma_{i\overline{p}} + \beta_{i\overline{p}}\epsilon_{i\overline{p}}, \tag{14c}$$

$$\text{with } \delta_p \geq 2\max_{p\in\Omega}(\kappa_p)\lambda_{\max}(S_p^{-1}) \geq 0, \tag{14d}$$

$$\text{and } \gamma_{ip}(t_0), \gamma_{i\overline{p}}(t_0) > \epsilon_{i\overline{p}}, \tag{14e}$$

where $S_p = S_p^T \in R^{n\times n}$, $\beta_{i\overline{p}}, \epsilon_{i\overline{p}} \in \mathbb{R}^+$ $i = 1, \cdots, n$ are static design parameters and t_0 is the initial time.

Remark 5. The adaptive laws (14) *are differential equations that let the proportional-derivative action of K_σ, L_σ adapt to unknown/changing power system parameters.*

3.2 Switching Laws

Define $\bar{\zeta}_M \triangleq \max_{p\in\Omega}\lambda_{\max}(P_p)$ and $\underline{\zeta}_m \triangleq \min_{p\in\Omega}\lambda_{\min}(P_p)$. Following *Definition 1*, an ADT switching is proposed with

$$\vartheta > \ln\mu/\chi, \tag{15}$$

where $\mu \triangleq \bar{\zeta}_M/\underline{\zeta}_m \geq 1$, $0 < \chi < \kappa$, with $\kappa \triangleq \min_{p\in\Omega}\{\kappa_p\}$.

Theorem 1. The closed-loop trajectories of power system (7) employing multi-area LFC (11), with adaptive law (14) and switching law (15) are UUB. An ultimate bound b on the tracking error $e(t)$ can be found as

$$b = \sqrt{\bar{\zeta}_M^{(N_0+1)}\mathcal{B}/\underline{\zeta}_m^{(N_0+2)}}, \tag{16}$$

$$\mathcal{B} = \max_{p\in\Omega}\left(\frac{\zeta_1}{\sqrt{\underline{\zeta}_m}(\kappa-\chi)} + \sqrt{\frac{\zeta_1^2}{\underline{\zeta}_m(\kappa-\chi)^2} + \frac{\zeta_2}{(\kappa-\chi)}}\right)^2. \tag{17}$$

where ς_1, ς_2 are detailed in the proof.

Proof. See Appendix.

Remark 6. The importance of Theorem 1 is in providing the first rigorous stability result for LFC with uncertainties, unmodelled dynamics and switching topologies. Theorem 1 involves the design of both adaptive and switching laws, both designs contributing to stability of the system.

4. SIMULATION RESULTS AND DISCUSSION

For easiness of providing all numerical values, let us use the three-area power system in Fig. 2 as a benchmark. For each area, the parameters are:

Area-1: $T_{p1} = 10,\ \frac{k_{p1}}{T_{p1}} = 0.1,\ R_1 = 0.05,\ T_1 = 2,\ B_1 = 41,\ k_1 = 0.5$

Area-2: $T_{p2} = 8,\ \frac{k_{p2}}{T_{p2}} = 0.083,\ R_2 = 0.05,\ T_2 = 5,\ B_2 = 81.5,\ k_2 = 0.5$

Area-3: $T_{p3} = 8,\ \frac{k_{p3}}{T_{p3}} = 0.063,\ R_3 = 0.05,\ T_3 = 8,\ B_3 = 62,\ k_3 = 0.5$

These parameters are used for simulation purposes, but unknown for control design. The switching topologies in Fig. 2 result in a switched power system as in (5) with

$$A_1 = \begin{bmatrix} 0 & 1 & 0 & 0 & 0 & 0 \\ -1.256 & -2.1 & 1.256 & 0 & 0 & 0 \\ 0 & 0 & 0 & 1 & 0 & 0 \\ 2.6062 & 0 & -5.2124 & -1.785 & 2.6062 & 0 \\ 0 & 0 & 0 & 0 & 0 & 1 \\ 0 & 0 & 3.165 & 0 & -3.165 & -1.385 \end{bmatrix}$$

$$A_2 = \begin{bmatrix} 0 & 1 & 0 & 0 & 0 & 0 \\ -2.512 & -2.1 & 1.256 & 0 & 1.256 & 0 \\ 0 & 0 & 0 & 1 & 0 & 0 \\ 2.6062 & 0 & -2.6062 & -1.785 & 0 & 0 \\ 0 & 0 & 0 & 0 & 0 & 1 \\ 3.165 & 0 & 0 & 0 & -3.165 & -1.385 \end{bmatrix}$$

$$A_3 = \begin{bmatrix} 0 & 1 & 0 & 0 & 0 & 0 \\ -1.256 & -2.1 & 0 & 0 & 1.256 & 0 \\ 0 & 0 & 0 & 1 & 0 & 0 \\ 0 & 0 & -2.6062 & -1.785 & 2.6062 & 0 \\ 0 & 0 & 0 & 0 & 0 & 1 \\ 3.165 & 0 & 3.165 & 0 & -6.330 & -1.385 \end{bmatrix}$$

$$A_4 = \begin{bmatrix} 0 & 1 & 0 & 0 & 0 & 0 \\ -2.512 & -2.1 & 1.256 & 0 & 1.256 & 0 \\ 0 & 0 & 0 & 1 & 0 & 0 \\ 2.6062 & 0 & -2.6062 & -1.785 & 2.6062 & 0 \\ 0 & 0 & 0 & 0 & 0 & 1 \\ 3.165 & 0 & 3.165 & 0 & -6.33 & -1.385 \end{bmatrix}$$

$$B = \begin{bmatrix} 0 & 0 & 0 \\ 0.1 & 0 & 0 \\ 0 & 0 & 0 \\ 0 & 0.083 & 0 \\ 0 & 0 & 0 \\ 0 & 0 & 0.063 \end{bmatrix}$$

For simplicity, let us choose a common reference model for all topologies, resulting from placing the closed-loop poles at the roots of $s^2 + 0.5\omega s + \omega^2$ with $\omega = 3.53 rad/s$:

$$A_{m\sigma} = \begin{bmatrix} 0 & 1 & 0 & 0 & 0 & 0 \\ -12.4609 & -4.9420 & 0 & 0 & 0 & 0 \\ 0 & 0 & 0 & 1 & 0 & 0 \\ 0 & 0 & -12.4609 & -4.9420 & 0 & 0 \\ 0 & 0 & 0 & 0 & 0 & 1 \\ 0 & 0 & 0 & 0 & -12.4609 & -4.9420 \end{bmatrix}$$

$$B_{m\sigma} = \begin{bmatrix} 0 & 0 & 0 \\ 12.4609 & 0 & 0 \\ 0 & 0 & 0 \\ 0 & 12.4609 & 0 \\ 0 & 0 & 0 \\ 0 & 0 & 12.4609 \end{bmatrix} \tag{18}$$

The solutions to (10) (unknown for control design) are

$$K_1^* = \begin{bmatrix} 112.0490 & -30.4200 & -12.5600 & 0 & 0 & 0 \\ -31.4000 & 0 & -87.3313 & -41.0482 & -31.4000 & 0 \\ 0 & 0 & -50.2381 & 0 & -147.5540 & -60.4286 \end{bmatrix}$$

$$K_2^* = \begin{bmatrix} -99.4890 & -30.4200 & -12.5600 & 0 & -12.5600 & 0 \\ -31.4000 & 0 & -118.7313 & -41.0482 & 0 & 0 \\ -50.2381 & 0 & 0 & 0 & -147.5540 & -60.4286 \end{bmatrix}$$

$$K_3^* = \begin{bmatrix} -112.0490 & -30.4200 & 0 & 0 & -12.5600 & 0 \\ 0 & 0 & -118.7313 & -41.0482 & -31.4000 & 0 \\ -50.2381 & 0 & -50.2381 & 0 & -97.3159 & -60.4286 \end{bmatrix}$$

$$K_4^* = \begin{bmatrix} -99.4890 & -30.4200 & -12.5600 & 0 & -12.5600 & 0 \\ -31.4000 & 0 & -118.7313 & -41.0482 & -31.4000 & 0 \\ -50.2381 & 0 & -50.2381 & 0 & -97.3159 & -60.4286 \end{bmatrix}$$

and $L_\sigma^* = diag(124.609, 149.590, 196.854)$ for all topologies. Note that A_σ and $A_{m\sigma}$ have the same block of integrators structure, and B and $B_{m\sigma}$ are block diagonal, so that the matching conditions (10) have solution.

Manuscript 554 submitted to 21st IFAC World Congress, 2020.
Received November 8, 2019.

Let $\kappa_1 = 0.25,\ \kappa_2 = 0.5,\ \kappa_3 = 0.4,\ \kappa_4 = 0.6,\ Q_i = 10I_{6\times 6}$ $\forall i$. Solving (13) gives the positive definite matrices:

$$P_1 = \begin{bmatrix} 25.4789 & 1.6792 & 0 & 0 & 0 & 0 \\ 1.6792 & 1.5472 & 0 & 0 & 0 & 0 \\ 0 & 0 & 25.4789 & 1.6792 & 0 & 0 \\ 0 & 0 & 1.6792 & 1.5472 & 0 & 0 \\ 0 & 0 & 0 & 0 & 25.4789 & 1.6792 \\ 0 & 0 & 0 & 0 & 1.6792 & 1.5472 \end{bmatrix}$$

$$P_2 = \begin{bmatrix} 28.4021 & 2.1107 & 0 & 0 & 0 & 0 \\ 2.1107 & 1.6963 & 0 & 0 & 0 & 0 \\ 0 & 0 & 28.4021 & 2.1107 & 0 & 0 \\ 0 & 0 & 2.1107 & 1.6963 & 0 & 0 \\ 0 & 0 & 0 & 0 & 28.4021 & 2.1107 \\ 0 & 0 & 0 & 0 & 2.1107 & 1.6963 \end{bmatrix}$$

$$P_3 = \begin{bmatrix} 27.1812 & 1.9282 & 0 & 0 & 0 & 0 \\ 1.9282 & 1.6332 & 0 & 0 & 0 & 0 \\ 0 & 0 & 27.1812 & 1.9282 & 0 & 0 \\ 0 & 0 & 1.9282 & 1.6332 & 0 & 0 \\ 0 & 0 & 0 & 0 & 27.1812 & 1.9282 \\ 0 & 0 & 0 & 0 & 1.9282 & 1.6332 \end{bmatrix}$$

$$P_4 = \begin{bmatrix} 29.6984 & 2.3079 & 0 & 0 & 0 & 0 \\ 2.3079 & 1.7643 & 0 & 0 & 0 & 0 \\ 0 & 0 & 29.6984 & 2.3079 & 0 & 0 \\ 0 & 0 & 2.3079 & 1.7643 & 0 & 0 \\ 0 & 0 & 0 & 0 & 29.6984 & 2.3079 \\ 0 & 0 & 0 & 0 & 2.3079 & 1.7643 \end{bmatrix}$$

Remark 7. Some components in K_σ^* corresponding to missing interconnection of the topology σ are 0 as a result of taking A_m in the same structure as A_σ. In addition, choosing a block diagonal A_m (feedback should reject couplings among areas) results in a block diagonal P_σ: this in turn allows the adaptive law (14) to implemented using only neighboring information in the topology σ, along the methodology in (Azzollini et al. (2018)).

The ADT constant resulting from (15) is $\vartheta = 7.6$. We consider the switching of Fig. 3, and design parameters for (14): $S_i = 100I_{3\times 3}$, $\delta_i = 0.08$, $\varepsilon_{i\overline{p}} = 0.2$, $\beta_{i\overline{p}} = 2\ \forall i$. The reference phase is $r(t) = [1 \quad 1 \quad 1]^T$, with time-varying load disturbance $[\Delta P_{d1} \quad \Delta P_{d2} \quad \Delta P_{d3}] = [-0.1\sin(0.5t) \quad 0.25\sin(0.1t) \quad 0.15\sin(0.2t)]$.

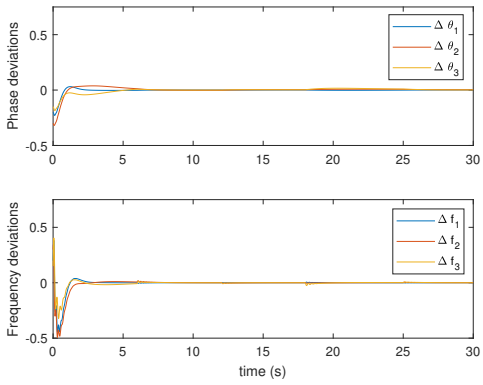

Fig. 4. Phase and frequency deviation for all 3 areas

A part from the initial phase, where the frequencies are initialized on purpose far from the equilibrium to highlight the regulation capabilities, Fig. 4 shows that $\Delta\theta$ and Δf are small around 0. Stability is achieved despite the switching topologies of Fig. 3, which cause negligible transients: the frequency deviations are inside ± 0.05 Hz even at switching instants. Stability is achieved in spite of load disturbance and unmodelled dynamics. Finally, Fig. 5 reveals how all control gains are automatically adapted to

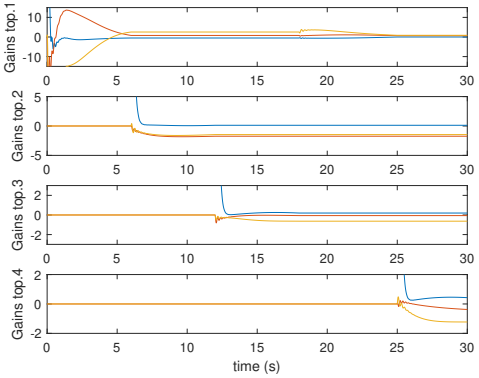

Fig. 5. Some adaptive control gains for the 4 topologies

cope with uncertainty and switching in the power system: when a new topology is activated, the gains rapidly adapt to keep the frequency around the equilibrium.

5. CONCLUSION

Although the need for an adaptive LFC system that dynamically weights its operation to adapt to changing circumstances is recognized in the power systems community, a formally stable adaptation framework around such idea was still missing. This work proposed a novel LFC framework in which provably stable adaptation can even handle changing topologies arising from reconfiguration against faults or switch among different control areas to dampen oscillations and face cyber-attacks.

Appendix A. STABILITY ANALYSIS PROOF

Proof. Law (14c) reveal that $\exists \underline{\gamma}_{i\sigma} \in \mathbb{R}^+$ such that

$$\underline{\gamma}_{i\sigma} \leq \gamma_{i\sigma}(t) \leq \bar{\gamma}_{i\sigma} \quad \forall t \geq t_0. \tag{A.1}$$

Stability relies on the Lyapunov candidate:

$$V = e^T(t)P_{\sigma(t)}e(t) + \sum_{s=1}^{N} \mathrm{tr}[\tilde{K}_s(t)M_s^{-1}\tilde{K}_s^T(t)] + \sum_{s=1}^{N} \mathrm{tr}[\tilde{L}_s^T(t)M_s^{-1}\tilde{L}_s(t)] + \sum_{s=1}^{N} \mathrm{tr}[\underline{\Gamma}_s\Gamma_s(t)]\}, \tag{A.2}$$

where $\underline{\Gamma}_\sigma = diag\{1/\underline{\gamma}_{i\sigma}\}$ and $M_\sigma = L_\sigma^* S_\sigma$. Analysis of (A.2) at the switching instants is required, since P_p is different for different topologies in general. Let topology $\sigma(t_{l+1}^-)$ be active when $t \in [t_l, t_{l+1})$ and topology $\sigma(t_{l+1})$ be active when $t \in [t_{l+1}, t_{l+2})$. Without the loss of generality, the behavior of $V(\cdot)$ is studied at the switching instant $t_{l+1}, l \in \mathbb{N}^+$: we have, before and after switching

$$V(t_{l+1}^-) = e^T(t_{l+1}^-)P_{\sigma(t_{l+1}^-)}e(t_{l+1}^-) + \sum_{s=1}^{N} \mathrm{tr}[\underline{\Gamma}_s(t_{l+1}^-)\Gamma_s(t_{l+1}^-)] + \sum_{s=1}^{N} \mathrm{tr}\left[\tilde{K}_s(t_{l+1}^-)M_s^{-1}\tilde{K}_s^T(t_{l+1}^-) + \tilde{L}_s^T(t_{l+1}^-)M_s^{-1}\tilde{L}_s(t_{l+1}^-)\right]$$

$$V(t_{l+1}) = e^T(t_{l+1})P_{\sigma(t_{l+1})}e(t_{l+1}) + \sum_{s=1}^{N} \mathrm{tr}[\underline{\Gamma}_s(t_{l+1}^-)\Gamma_s(t_{l+1})] + \sum_{s=1}^{N} \mathrm{tr}\left[\tilde{K}_s(t_{l+1})M_s^{-1}\tilde{K}_s^T(t_{l+1}) + \tilde{L}_s^T(t_{l+1})M_s^{-1}\tilde{L}_s(t_{l+1})\right]$$

Manuscript 554 submitted to 21st IFAC World Congress, 2020.
Received November 8, 2019.

Continuity of the tracking error $e(\cdot)$ in (12) and the gains updated via (14), give $e(t_{l+1}^-) = e(t_{l+1}), \tilde{K}_s(t_{l+1}^-) = \tilde{K}_s(t_{l+1}), \tilde{L}_s(t_{l+1}^-) = \tilde{L}_s(t_{l+1})$, and $\Gamma_s(t_{l+1}^-) = \Gamma_s(t_{l+1})$ for any switching law. Due to $e^T(t)P_pe(t) \leq \bar{\zeta}_M e^T(t)e(t)$, and $e^T(t)P_pe(t) \geq \underline{\zeta}_m e^T(t)e(t)$ we have

$$V(t_{l+1}) - V(t_{l+1}^-) = e^T(t_{l+1}^-)(P_{\sigma(t_{l+1})} - P_{\sigma(t_{l+1}^-)})e(t_{l+1}^-)$$
$$\leq \frac{\bar{\zeta}_M - \underline{\zeta}_m}{\underline{\zeta}_m} V(t_{l+1}^-) \Rightarrow V(t_{l+1}) \leq \mu V(t_{l+1}^-) \tag{A.3}$$

with $\mu \triangleq \bar{\zeta}_M/\underline{\zeta}_m \geq 1$. Next, the behavior of $V(t)$ is studied between two consecutive switching instants, $t \in [t_l \;\; t_{l+1})$. Let $\sigma(t) = p$ denote the active topology and $\overline{p}$ an inactive one. Using (13), (12) and (14a)-(14c) we have

$$\dot{V} \leq -e^T(1+\kappa_p)P_pe + 2e^TP_p(B(\tilde{K}_px + (\tilde{L}_p + \Gamma_p)r) + 2d)$$
$$+ 2\sum_{s=1}^{N}\big\{\operatorname{tr}[\tilde{K}_sM_s^{-1}\dot{K}_s^T] + \operatorname{tr}[\tilde{L}_s^TM_s^{-1}\dot{L}_s] + \operatorname{tr}[\underline{\Gamma}_s\dot{\Gamma}_s]\big\}$$
$$\leq -\kappa_pe^TP_pe + 2e^TP_pB\Gamma_pr + d^TP_pd + \sum_{\overline{p}\in\mathcal{I}(p)}\operatorname{tr}[\underline{\Gamma}_{\overline{p}}\dot{\Gamma}_{\overline{p}}]$$
$$- 2\operatorname{tr}[\tilde{K}_p\delta_pL_p^{*-1}K_p^T] - 2\operatorname{tr}[\tilde{L}_p^T\delta_pL_p^{*-1}L_p]. \tag{A.4}$$

Using Young's inequality, we have

$$-2\operatorname{tr}[\tilde{K}_p\delta_pL_p^{*-1}K_p^T] < -\operatorname{tr}[\tilde{K}_p\delta_pL_p^{*-1}\tilde{K}_p^T]$$
$$+ \operatorname{tr}[K_p^*\delta_pL_p^{*-1}K_p^{*T}], \tag{A.5}$$

(and similar for $\tilde{L}_p$) where the inequalities rely on the fact that L_σ^* is a diagonal positive definite matrix. Further, noting $\underline{\Gamma}_{\overline{p}}\dot{\Gamma}_{\overline{p}} = diag\{\dot{\gamma}_{i\overline{p}}/\underline{\gamma}_{i\overline{p}}\}$, $i = 1, \cdots, m$, the following can be deduced from (14c) and (A.1)

$$\frac{\dot{\gamma}_{i\overline{p}}}{\underline{\gamma}_{i\overline{p}}} = \frac{-\left(\beta_{i\overline{p}} + \delta_{\overline{p}}\left(\{K_{\overline{p}}K_{\overline{p}}{}^T\}_{ii} + \{L_{\overline{p}}^TL_{\overline{p}}\}_{ii}\right)\right)\gamma_{i\overline{p}} + \beta_{i\overline{p}}\epsilon_{i\overline{p}}}{\underline{\gamma}_{i\overline{p}}}$$
$$\leq -\delta_{\overline{p}}\left(\{K_{\overline{p}}K_{\overline{p}}^T\}_{ii} + \{L_{\overline{p}}^TL_{\overline{p}}\}_{ii}\right) + \frac{\beta_{i\overline{p}}\epsilon_{i\overline{p}}}{\underline{\gamma}_{i\overline{p}}}. \tag{A.6}$$

Moreover, Young's inequality yield

$$\operatorname{tr}[\tilde{K}_\sigma\tilde{K}_\sigma^T] = \operatorname{tr}[K_\sigma K_\sigma^T - 2K_\sigma K_\sigma^{*T} + K_\sigma^*K_\sigma^{*T}]$$
$$\leq 2\operatorname{tr}[K_\sigma K_\sigma^T + K_\sigma^*K_\sigma^{*T}]. \tag{A.7}$$

(similar for $\tilde{L}_\sigma$). Using (A.5)-(A.7), (A.4) is simplified as

$$\dot{V} \leq -\kappa_pV + 2e^TP_pB\Gamma_pr + d^TP_pd$$
$$+ \operatorname{tr}[\tilde{K}_p^TL_p^{*-1}\tilde{K}_p(\kappa_p\lambda_{\max}(S_p^{-1}) - \delta_p)] + \operatorname{tr}[K_p^{*T}\delta_pL_p^{*-1}K_p^*]$$
$$+ \operatorname{tr}[\tilde{L}_p^TL_p^{*-1}\tilde{L}_p(\kappa_p\lambda_{\max}(S_p^{-1}) - \delta_p)] + \operatorname{tr}[L_p^{*T}\delta_pI_n]$$
$$+ \sum_{\overline{p}\in\mathcal{I}(p)}\Big(\operatorname{tr}[\tilde{K}_{\overline{p}}^TL_{\overline{p}}^{*-1}\tilde{K}_{\overline{p}}(\kappa_{\overline{p}}\lambda_{\max}(S_{\overline{p}}^{-1}) - \frac{1}{2}\delta_{\overline{p}})]\Big) + \frac{1}{2}\operatorname{tr}[K_{\overline{p}}^{*T}\delta_{\overline{p}}K_{\overline{p}}^*]$$
$$+ \sum_{\overline{p}\in\mathcal{I}(p)}\Big(\operatorname{tr}[\tilde{L}_{\overline{p}}^TL_{\overline{p}}^{*-1}\tilde{L}_{\overline{p}}(\kappa_{\overline{p}}\lambda_{\max}(S_{\overline{p}}^{-1}) - \frac{1}{2}\delta_{\overline{p}})]\Big) + \frac{1}{2}\operatorname{tr}[L_{\overline{p}}^{*T}\delta_{\overline{p}}L_{\overline{p}}^*]$$
$$+ \sum_{s=1}^{N}\operatorname{tr}[\kappa_s\underline{\Gamma}_s\Gamma_s] + \sum_{\overline{p}\in\mathcal{I}(p)}\sum_{i=1}^{m}(\beta_{i\overline{p}}\epsilon_{i\overline{p}})/\underline{\gamma}_{i\overline{p}}$$
$$\leq -\kappa V + 2||e||||P_pB\Gamma_pr|| + \bar{\zeta}_M||d||^2 + \sum_{s=1}^{N}\operatorname{tr}[\kappa_s\underline{\Gamma}_s\Gamma_s]$$
$$+ \operatorname{tr}[K_p^{*T}\delta_pL_p^{*-1}K_p^*] + \operatorname{tr}[L_p^{*T}\delta_pI_n]$$
$$+ \sum_{\overline{p}\in\mathcal{I}(p)}\sum_{i=1}^{m}\Big(\frac{1}{2}\operatorname{tr}[K_{\overline{p}}^{*T}\delta_{\overline{p}}K_{\overline{p}}^*] + \frac{1}{2}\operatorname{tr}[L_{\overline{p}}^{*T}\delta_{\overline{p}}L_{\overline{p}}^*] + \frac{\beta_{i\overline{p}}\epsilon_{i\overline{p}}}{\underline{\gamma}_{i\overline{p}}}\Big). \tag{A.8}$$

By definition $r(t) \in \mathcal{L}_\infty$ and by design $\Gamma_s \in \mathcal{L}_\infty$ from (A.1). Therefore, $\exists\zeta_1 \in \mathbb{R}^+$ such that $||P_pB\Gamma_pr|| \leq \zeta_1, \; \forall p \in \Omega$. Further we define a scalar ζ_2 as

$$\zeta_2 \triangleq \bar{\varrho}_M||d||^2 + \max_{p\in\Omega}(\operatorname{tr}[K_p^{*T}\delta_pK_p^*] + \operatorname{tr}[L_p^{*T}\delta_pL_p^*])$$
$$\sum_{\overline{p}\in\mathcal{I}(p)}\sum_{i=1}^{m}\Big(\frac{1}{2}\operatorname{tr}[K_{\overline{p}}^{*T}\delta_{\overline{p}}K_{\overline{p}}^*] + \frac{1}{2}\operatorname{tr}[L_{\overline{p}}^{*T}\delta_{\overline{p}}L_{\overline{p}}^*] + \frac{\beta_{i\overline{p}}\epsilon_{i\overline{p}}}{\underline{\gamma}_{i\overline{p}}}\Big)$$
$$+ \sum_{s=1}^{N}\operatorname{tr}[\kappa_s\underline{\Gamma}_s\Gamma_s]. \tag{A.9}$$

Again, the definition of the Lyapunov function (A.2) yields

$$V \geq \lambda_{\min}(P_p)||e||^2 \geq \underline{\varrho}_m||e||^2. \tag{A.10}$$

We had defined earlier $0 < \kappa < \zeta$. Hence, using (A.9)-(A.10), (A.8) is simplified as

$$\dot{V} \leq -\chi V - (\kappa - \chi)V + 2\zeta_1\sqrt{V/\underline{\zeta}_m} + \zeta_2. \tag{A.11}$$

Thus, $\dot{V} \leq -\chi V$ is established when

$$V \geq \max_{p\in\Omega}\left(\frac{\zeta_1}{\sqrt{\underline{\zeta}_m}(\kappa-\chi)} + \sqrt{\frac{\zeta_1^2}{\underline{\zeta}_m(\kappa-\chi)^2} + \frac{\zeta_2}{(\kappa-\chi)}}\right)^2 = \mathcal{B}.$$

So we obtain that a positive $\mathcal{B}$ as (17).

In light of this, further analysis is needed to observe the behaviour of $V(t)$ between the two consecutive switching intervals, i.e., $t \in [t_l \;\; t_{l+1})$, for two possible cases:

- **(i)** when $V(t) \geq \mathcal{B}$, we have $\dot{V}(t) \leq -\chi V(t)$ from (A.11) implying exponential decrease of $V(t)$;
- **(ii)** when $V(t) < \mathcal{B}$, $V(t)$ may increase.

Behaviour of $V(t)$ is discussed below individually for these two cases.

Case (i): There exists a time, call it T_1, when $V(t)$ enters into the bound $\mathcal{B}$ and $N_1(t)$ denotes the number of intervals a topology p, $p \in \Omega$ remains active for $t \in [t_l \;\; t_l + T_1)$. Accordingly, for $t \in [t_l \;\; t_l + T_1)$, using (A.3), (A.11) and $N_\sigma(t_l, t)$ from Definition 1 we have

$$V(t) \leq \exp\left(-\chi(t - t_{N_1(t)-1})\right)V(t_{N_1(t)-1})$$
$$\leq \mu\exp\left(-\chi(t - t_{N_1(t)-1})\right)V(t_{N_1(t)-1}^-)$$
$$\leq \mu\exp\left(-\chi(t - t_{N_1(t)-1})\right)$$
$$\times \mu\exp\left(-\chi(t_{N_1(t)-1} - t_{N_1(t)-2})\right)V(t_{N_1(t)-2}^-)$$
$$\vdots$$
$$= \mu^{N_\sigma(t_0,t)}\exp\left(-\chi(t - t_0)\right)V(t_0)$$
$$= c\left(\exp\left(-\chi + (\ln\mu/\vartheta)(t - t_0)\right)\right)V(t_0), \tag{A.12}$$

where $c \triangleq \exp\left(N_0\ln\mu\right)$ is a constant. Substituting the ADT condition $\vartheta > \ln\mu/\chi$ in (A.12) yields $V(t) < cV(t_0)$ for $t \in [t_l \;\; t_l + T_1)$. Moreover, as $V(t_l + T_1) < \mathcal{B}$, one has $V(t_{N_1(t)+1}) < \mu\mathcal{B}$ from (A.3) at the next switching

instant $t_{N_1(t)+1}$ after $t_l + T_1$. Along the lines of (Yuan et al. (2018)), one has that once $V(t)$ enters the interval $[0, \mathcal{B}]$, it cannot exceed the bound $c\mu\mathcal{B}$ any time later with the ADT switching law (15).

Case (ii): It can be easily verified that the same argument below (A.12) also holds for Case (ii).

Thus, observing the stability arguments of the Cases (i) and (ii), it can be concluded that the closed-loop system remains GUUB already stated in theorem statement. Further, based on this analysis, we have

$$V(t) \leq \max\{cV(t_0), c\mu\mathcal{B}\}, \quad \forall t \geq t_0. \tag{A.13}$$

Again, the definition of the Lyapunov function (A.2) yields

$$V(t) \geq \lambda_{\min}(P_{\sigma(t)})\|e(t)\|^2 \geq \underline{\zeta}_m\|e(t)\|^2. \tag{A.14}$$

Using (A.13) and (A.14) we have

$$\|e(t)\|^2 \leq \frac{1}{\underline{\zeta}_m}\max\{cV(t_0), c\mu\mathcal{B}\}, \quad \forall t \geq t_0. \tag{A.15}$$

Therefore, substituting $c = \exp(N_0 \ln \mu)$ and $\mu = \bar{\zeta}_M/\underline{\zeta}_m$ into (A.15) and using the expression of $\mathcal{B}$ from (17), leading to ultimate bound b on the tracking error e can be found as (16).

REFERENCES

Abazari, A., Monsef, H., and Wu, B. (2019). Coordination strategies of distributed energy resources including fess, deg, fc and wtg in load frequency control (lfc) scheme of hybrid isolated micro-grid. *Int. J. Electr. Power Energy Syst.*, 109, 535 – 547.

Azzollini, I.A., Baldi, S., and Kosmatopoulos, E.B. (2018). Adaptive synchronization in networks with heterogeneous uncertain kuramoto-like units. In *2018 European Control Conference (ECC)*, 2417–2422.

Boonchuay, C. (2014). Improving regulation service based on adaptive load frequency control in lmp energy market. *IEEE Trans. Power Syst.*, 29(2), 988–989.

DeLellis, P., Di Bernardo, M., Gorochowski, T.E., and Russo, G. (2010). Synchronization and control of complex networks via contraction, adaptation and evolution. *IEEE Circuits and Systems Magazine*, 10(3), 64–82.

Dey, R., Ghosh, S., Ray, G., and Rakshit, A. (2012). $\mathcal{H}_\infty$ load frequency control of interconnected power systems with communication delays. *Int. J. Electr. Power Energy Syst.*, 42(1), 672 – 684.

Doolla, S. and Bhatti, T.S. (2006). Load frequency control of an isolated small-hydro power plant with reduced dump load. *IEEE Trans. Power Syst.*, 21(4), 1912–1919.

Ersdal, A.M., Imsland, L., and Uhlen, K. (2016). Model predictive load-frequency control. *IEEE Trans. Power Syst.*, 31(1), 777–785.

Fan, L., Miao, Z., and Osborn, D. (2009). Wind farms with hvdc delivery in load frequency control. *IEEE Trans. Power Syst.*, 24(4), 1894–1895.

Hanwate, S., Hote, Y.V., and Saxena, S. (2018). Adaptive policy for load frequency control. *IEEE Trans. Power Syst.*, 33(1), 1142–1144.

Hespanha, J.P. and Morse, A.S. (1999). Stability of switched systems with average dwell-time. In *Proceedings of the 38th IEEE Conference on Decision and Control*, volume 3, 2655–2660. IEEE.

Korkas, C.D., Baldi, S., Michailidis, I., and Kosmatopoulos, E.B. (2015). Intelligent energy and thermal comfort management in grid-connected microgrids with heterogeneous occupancy schedule. *Applied Energy*, 149, 194 – 203.

Liu, T., Hill, D.J., and Zhang, C. (2016). Non-disruptive load-side control for frequency regulation in power systems. *IEEE Transactions on Smart Grid*, 7(4), 2142–2153.

Mahmoud, M.S., Hamdan, M.M., and Baroudi, U.A. (2019). Modeling and control of cyber-physical systems subject to cyber attacks: A survey of recent advances and challenges. *Neurocomputing*, 338, 101 – 115.

Mallada, E., Zhao, C., and Low, S. (2017). Optimal load-side control for frequency regulation in smart grids. *IEEE Transactions on Automatic Control*, 62(12), 6294–6309.

Mu, C., Tang, Y., and He, H. (2017). Improved sliding mode design for load frequency control of power system integrated an adaptive learning strategy. *IEEE Trans. Ind. Electron.*, 64(8), 6742–6751.

Polajžer, B., Petrun, M., and Ritonja, J. (2018). Adaptation of load-frequency-control target values based on the covariances between area-control errors. *IEEE Trans. Power Syst.*, 33(6), 5865–5874.

Prostejovsky, A.M., Marinelli, M., Rezkalla, M., Syed, M.H., and Guillo-Sansano, E. (2018). Tuningless load frequency control through active engagement of distributed resources. *IEEE Trans. Power Syst.*, 33(3), 2929–2939.

Roy, S., Patel, A., and Kar, I.N. (2018). Analysis and design of a wide-area damping controller for inter-area oscillation with artificially induced time delay. *IEEE Transactions on Smart Grid*.

Saxena, S. and Hote, Y.V. (2013). Load frequency control in power systems via internal model control scheme and model-order reduction. *IEEE Trans. Power Syst.*, 28(3), 2749–2757.

Schiffer, J., Dorfler, F., and Fridman, E. (2017). Robustness of distributed averaging control in power systems: Time delays & dynamic communication topology. *Automatica*, 80, 261 – 271.

Tao, G. (2014). Multivariable adaptive control: A survey. *Automatica*, 50(11), 2737–2764.

Yousef, H.A., AL-Kharusi, K., Albadi, M.H., and Hosseinzadeh, N. (2014). Load frequency control of a multi-area power system: An adaptive fuzzy logic approach. *IEEE Trans. Power Syst.*, 29(4), 1822–1830.

Yousef, H. (2015). Adaptive fuzzy logic load frequency control of multi-area power system. *Int. J. Electr. Power Energy Syst.*, 68, 384 – 395.

Yuan, S., Schutter, B.D., and Baldi, S. (2018). Robust adaptive tracking control of uncertain slowly switched linear systems. *Nonlinear Analysis: Hybrid Systems*, 27, 1–12.

Zhang, C., Liu, T., and Hill, D.J. (2019). Switched distributed load-side frequency control of power systems. *Int. J. Electr. Power Energy Syst.*, 105, 709 – 716.

Zhao, C., Topcu, U., Li, N., and Low, S. (2014). Design and stability of load-side primary frequency control in power systems. *IEEE Transactions on Automatic Control*, 59(5), 1177–1189.